

## NANO EXPRESS

## Open Access

# First-principles investigation on the segregation of Pd at $\text{LaFe}_{1-x}\text{Pd}_x\text{O}_{3-y}$ surfaces

Zhi-xue Tian<sup>1</sup>, Akifumi Uozumi<sup>2</sup>, Ikutaro Hamada<sup>3</sup>, Susumu Yanagisawa<sup>4</sup>, Hidetoshi Kizaki<sup>1</sup>, Kouji Inagaki<sup>1</sup> and Yoshitada Morikawa<sup>1,5\*</sup>**Abstract**

First-principles calculations were performed to investigate the effect of Pd concentration and oxygen vacancies on the stability of Pd at  $\text{LaFeO}_3$  surfaces. We found a much stronger tendency of Pd to segregate by taking the aggregation of Pd at  $\text{LaFe}_{1-x}\text{Pd}_x\text{O}_{3-y}$  surfaces into consideration, resulting in a pair of Pd-Pd around a vacancy. Moreover, we predicted that one oxygen-vacancy-containing  $\text{FeO}_2$ -terminated surfaces would be stable at high temperatures by comparing the stability of  $\text{LaFe}_{1-x}\text{Pd}_x\text{O}_{3-y}$  surfaces, which further supports our previous conclusion that a Pd-containing perovskite catalyst should be calcined at 1,073 K or higher temperatures in air to enhance the segregation of Pd in the vicinity of surfaces to rapidly transform the Pd catalyst from oxidized to reduced states on the perovskite support.

**Keywords:** Perovskite,  $\text{LaFeO}_3$ , Palladium, Density functional theory, Surface segregation

**Background**

A three-way catalyst simultaneously transforms toxic exhaust emissions from motor vehicles into harmless gases. However, the sintering problem, i.e., the growth and agglomeration of precious metal particles on conventional catalysts during vehicle use dramatically degrades catalytic activity, and large amounts of precious metals are required to retain the activity of catalysts after long periods of use. Thus, intelligent catalysts have attracted worldwide attention due to their greatly improved durability as a result of the self-regenerative function of precious metal nanoparticles [1-3]. It has been confirmed that the activity of catalysts can be preserved, and the amount of precious metals that are required can be reduced by 70% to 90% [4,5]. The self-regenerative function, which can be explained as resulting from the transformation of the state of precious metals (Pd, Pt, and Rh) that reversibly move into and out of the  $\text{LaFe}_{1-x}\text{M}_x\text{O}_3$  perovskite lattice,

significantly suppresses the growth of precious metals during the use of catalysts.

Thus far, many experiments have been devoted to research on the state of Pd in perovskite in redox processes. Uenishi et al. [6] investigated the superior start-up activity of  $\text{LaFePdO}_x$  at low temperatures (from 100°C to 400°C) using X-ray spectroscopic techniques under the practical conditions where they controlled automotive emissions. They found the  $\text{Pd}^0$  phase partially segregated outside the surface even at low temperatures; thus, the segregation of  $\text{Pd}^0$  under a reductive atmosphere induced the start-up activity of  $\text{LaFePdO}_x$ . Eyssler et al. found a high concentration of Pd distributed on the  $\text{LaFeO}_3$  (LFO) surface that contributed to high methane combustion due to the formation of  $\text{PdO}$  in which  $\text{Pd}^{2+}$  was in square planar coordination. Additionally, two Pd species ( $\text{Pd}^{2+}$  at the surface and  $\text{Pd}^{3+}$  in a solid solution) were found to be generated in further calcination.  $\text{Pd}^{2+}$  and  $\text{Pd}^{3+}$  could be transformed in equilibrium under thermal treatment conditions [7,8]. More recently, Eyssler et al. studied the state of Pd in different B-site substitutions and compared the effect of catalytic activities on methane combustion. A well-dispersed octahedral Pd-O species was found for Fe- and Co B- site cations, and  $\text{PdO}$  particles were on the  $\text{LaMnO}_3$  surface [9]. Above all, related investigations have become more important as the activity of

\* Correspondence: [morikawa@prec.eng.osaka-u.ac.jp](mailto:morikawa@prec.eng.osaka-u.ac.jp)<sup>1</sup>Division of Precision Science & Technology and Applied Physics, Graduate School of Engineering, Osaka University, 2-1, Yamada-oka Suita, Osaka 565-0871, Japan<sup>5</sup>Elements Strategy Initiative for Catalysts and Batteries (ESICB), Kyoto University, Katsura, Kyoto 615-8520, Japan

Full list of author information is available at the end of the article

catalysts strongly depends on the state of the precipitated Pd.

Hamada et al. [10] more recently found in a density functional theory (DFT) investigation that oxygen vacancies ( $V_O$ s) that formed near the LFO surface promoted the segregation of Pd. They also proposed a scenario that perovskite containing precious metal is calcined during the catalyst preparation step at 1,073 K for 2 h in air, and then  $V_O$ s are produced that enhance Pd segregation, resulting in a  $\text{LaPdO}_{3-y}$  layer that eventually forms close to the surface. The  $\text{LaPdO}_{3-y}$  layer in the vicinity of the surface promotes efficient switching between Pd metal particles under reductive conditions and the dissolved state of Pd in the  $\text{LaFe}_{1-x}\text{Pd}_x\text{O}_3$  perovskite lattice under oxidative conditions. Therefore, the  $\text{LaPdO}_{3-y}$  layers formed in the vicinity of the oxide surface play a key role in the self-regenerative function. Almost simultaneously, transmission electron microscopy observations [11] of atomic-scale processes in Pd-LFO catalysts have demonstrated that redox reactions between the formation of Pd particles on the Pd-LFO surface under reducing conditions and the dissolution of Pd particles into LFO under oxidizing conditions take place in spatially-limited areas, especially in the proximity of oxide surfaces, indicating strong interactions between Pd and oxide surfaces. Katz's results also provided strong support for the mechanism proposed by Hamada et al. However, the stability of the  $\text{LaPdO}_{3-y}$  layer and the mechanism for Pd leaving the  $\text{LaPdO}_{3-y}$  layer have not been discussed in detail. The interaction between Pd atoms in the perovskite host is especially important considering the possibility of nanoscale spinodal decomposition as pointed out by Kizaki et al. [12]. Therefore, we systemically studied the relative stability of the  $\text{Pd}_m\text{V}_{On}$ -containing surfaces ( $m = 1$  and  $2$  and  $n = 0, 1$ , and  $2$ ) in our present work to investigate possible phases appearing in steps to prepare catalysts at high temperature in air.

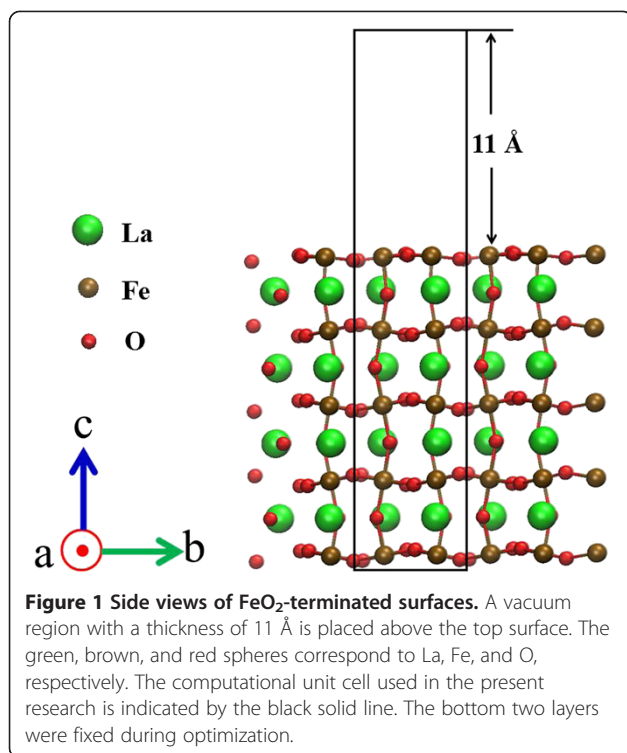
## Methods

### Model and computation

We have calculated the lattice constants [13] of LFO and the segregation tendency of Pd at two terminations of the perovskite surfaces with and without  $V_O$  by using state [14,15] and quantum ESPRESSO (QE) [16] codes. We found that both state and QE codes yielded the similar bulk lattice constants and caused the segregation behavior of Pd, which was a strong indication that both codes could admirably describe the properties of Pd incorporated in the  $\text{LaFe}_{1-x}\text{Pd}_x\text{O}_{3-y}$  surfaces. Here, we employed the state code to do the first-principles calculations. The ion-electron interactions were described using ultrasoft pseudopotentials [17], and the exchange and correlation potential was represented by

a generalized gradient approximation (GGA) in the Perdew-Burke-Ernzerhof formula [18]. DFT calculations with Hubbard correction (DFT+U) are known to correct the bandgap and magnetic moment in local-density approximation and generalized gradient approximation calculations. This method can yield reasonable agreement with the experimental results. We omitted DFT+U from this work because Hamada et al. verified [10] that electronic structures with DFT+U are qualitatively the same as those in GGA calculations, and they have not changed their conclusions. However, since the relative energies that are used to determine the stability of perovskite surfaces might be influenced by the exchange and correlation potential, even though DFT+U fails to give better results than GGA calculations to predict the phase stability of hematite surfaces [19], we still intend to investigate the effect of DFT+U in later work. The original unit cell used to construct the LFO perovskite surface was a  $\text{GdFeO}_3$ -type orthorhombic unit cell (adapted from Figure one in [13]), in which the local magnetic moments of Fe are aligned in G-type anti-ferromagnetic order. The relaxed lattice constants for  $a$ ,  $b$ , and  $c$  in bulk LFO correspond to 0.575, 0.559, and 0.792 nm, respectively, which are in reasonable agreement with the experimental values [20] of 0.558, 0.556, and 0.785 nm. The cutoff energies for the wave function and augmentation charge density are 25 Ry for the former and 225 Ry for the latter.

We modeled the  $\sqrt{2} \times \sqrt{2}$  LFO (001) surface by using a repeated slab model. Hamada et al. [10] had already shown and we confirmed [13] that one  $V_O$  formed in the LFO (001) surface promoted the tendency of Pd to segregate in bulk. Moreover, we further demonstrated that Pd has the strongest tendency to segregate at  $\text{FeO}_2$ -terminated surfaces containing  $V_O$ s, in comparison with three other surfaces, i.e., LaO-terminated surfaces with and without  $V_O$ s and the perfect  $\text{FeO}_2$ -terminated surfaces. Additionally, Lee et al. [21] calculated a surface phase diagram of the LFO (010) surface and argued that the LaO-terminated surface could be predicted to be stable at lower temperature (773 K), which was in agreement with the previous experimental results measured by X-ray photoelectron spectra [22,23]. In contrast, the  $\text{FeO}_2$ -terminated surface became dominant at high temperatures (>1,500 K). Therefore, thermal treatment at high temperature is essential to make  $\text{FeO}_2$ -terminated surfaces more stable. We thus examined  $\text{FeO}_2$ -terminated surfaces in this work. The atomic configuration for a pristine  $\text{FeO}_2$ -terminated surface is in Figure 1, which was obtained with visual molecular dynamics [24]. Our repeated slab model consisted of nine atomic layers, i.e., five  $\text{FeO}_2$  layers and four LaO layers. Further, one unit cell contained eight La atoms, 10 Fe atoms, and 28 O atoms in total. Brillouin-zone



integration was carried out within a Monkhorst-Pack [25] scheme using a uniform ( $4 \times 4 \times 1$ ) mesh. We inserted a vacuum region of 11 Å to minimize the interaction between two adjacent slabs. We fixed the two bottom layers to the bulk coordinates during the geometry optimizations and allowed atomic relaxation for the rest of the layers.

## Results and discussion

Simplified 2D tables that represent the complicated atomic configurations of perovskite surfaces have been provided in Figure 2 to clarify the discussion. Configurations with negative formation energies are more stable than the reference configuration. One Pd segregating from the third  $\text{FeO}_2$  layer to the surface just releases an energy of about 0.08 eV [13] (Figure 2 group I (a) and (b)) as we demonstrated without  $\text{V}_{\text{O}}$ s. However, when one Pd has already segregated on the topmost site of a perfect LFO surface, the additional Pd prefers to stay inside the bulk rather than segregate onto the surface as shown in Figures 2 group I (c) to (e). One first has to determine the positions of  $\text{V}_{\text{O}}$ s and Pd atoms in studying the effect induced by  $\text{V}_{\text{O}}$ s on the stability of Pd atoms. We have to calculate all the possible configurations containing  $\text{V}_{\text{O}}$ s and Pd. Hamada et al. [10] pointed out

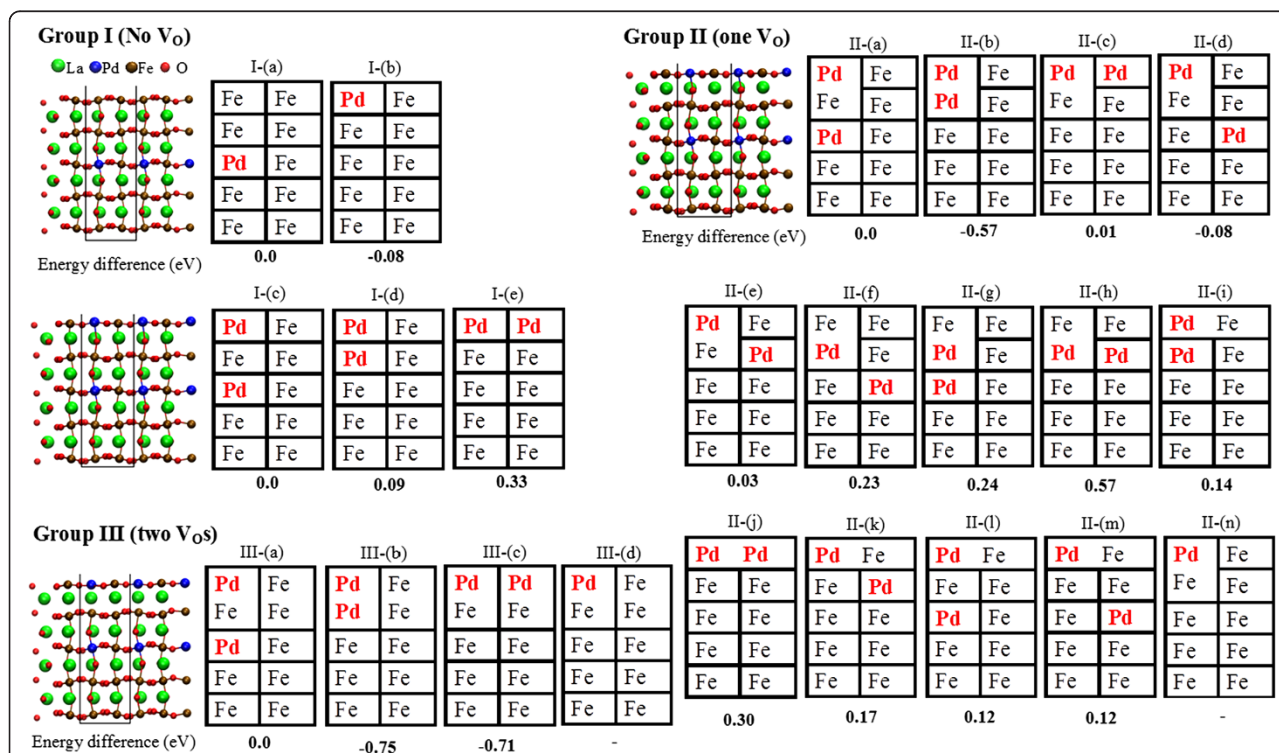


**Figure 2** Simplified 2D tables that represent complicated structures of perovskite surfaces containing  $\text{Pd}_n$  ( $n=1$  and 2). Groups I to III are for the geometries with no  $\text{V}_{\text{O}}$ , one  $\text{V}_{\text{O}}$ , and two  $\text{V}_{\text{O}}$ s, respectively. The atomic configurations for each group, which are schematically represented by the table of panel (a), are indicated by the ball and stick model. The uncapping unit cell is indicated by the black line as seen in Figure 1. The rows containing Fe (Pd) in each table represent  $\text{FeO}_2$  ( $\text{PdO}_2$ ) layers, and the vertical lines represent O atoms in  $\text{FeO}_2$  ( $\text{PdO}_2$ ) layers. The horizontal lines represent O atoms in LaO layers (La atoms are not explicitly shown). The absence of vertical (horizontal) lines means  $\text{V}_{\text{O}}$  forming at the surface (subsurface) site. The calculated difference in energy (in eV) for each panel relative to the total energy of the surface in panel (a) is also listed.

that the most stable site for  $V_O$  is the topmost surface for pristine LFO and the subsurface (LaO layer) O site for Pd located in the first layer of the LFO surface. We considered  $V_O$ s formed at those two possible sites along with various configurations of Pd atoms at the  $FeO_2$ -terminated surface. We set the first configuration in panel (a) in group II to the reference state in which one Pd atom was located in the first  $FeO_2$  layer, the second Pd atom was in the third  $FeO_2$  layer, and a  $V_O$  was located in the first LaO layer just under the first Pd. The positions of the first Pd atom and  $V_O$  were found to have the most stable configuration. Positive formation energies for panels (i) to (m) in group II indicate that  $V_O$ s that formed on the topmost surface is unstable. However, the most stable state was found with a formation energy of about -0.57 eV when a  $V_O$  was located at the subsurface nearly at the center of two Pd atoms, as seen in Figure 2 group II (b). However, one of the Pd

atoms tended to be buried in the second  $FeO_2$  layer (panel (b)) rather than exposed to the vacuum (panel (c) in group II), and the energy discrepancy between panels (b) and (c) was as large as 0.58 eV. We analyzed the projected density of state (PDOS) of the two Pd atoms in the  $V_O$ -containing surfaces to understand the origin for the difference in stability between panels group II (b) and (c). All the results are presented in Figure 3. We denoted the Pd located at the top-left site in the unit cell in Figure 2 group II (a) to (c) as Pd-1 and the other one as Pd-2. Where Pd-2 stayed inside the bulk (Figure 2 group II (a)), the PDOS of Pd-1 looked similar to that in Figure five (e) in [13], i.e., a single Pd at the first  $FeO_2$  layer with one  $V_O$  beneath it. The  $V_O$  beneath Pd-1 reduces hybridization between the Pd  $d_{3z^2}$  state and O  $p$  state, leading to significant stabilization of the  $d_{3z^2}$  state. The degenerated  $e_g$  states of 4d-orbitals for Pd-2 are singly occupied (Figure 3a<sub>2</sub>). When Pd-2 replaces the Fe

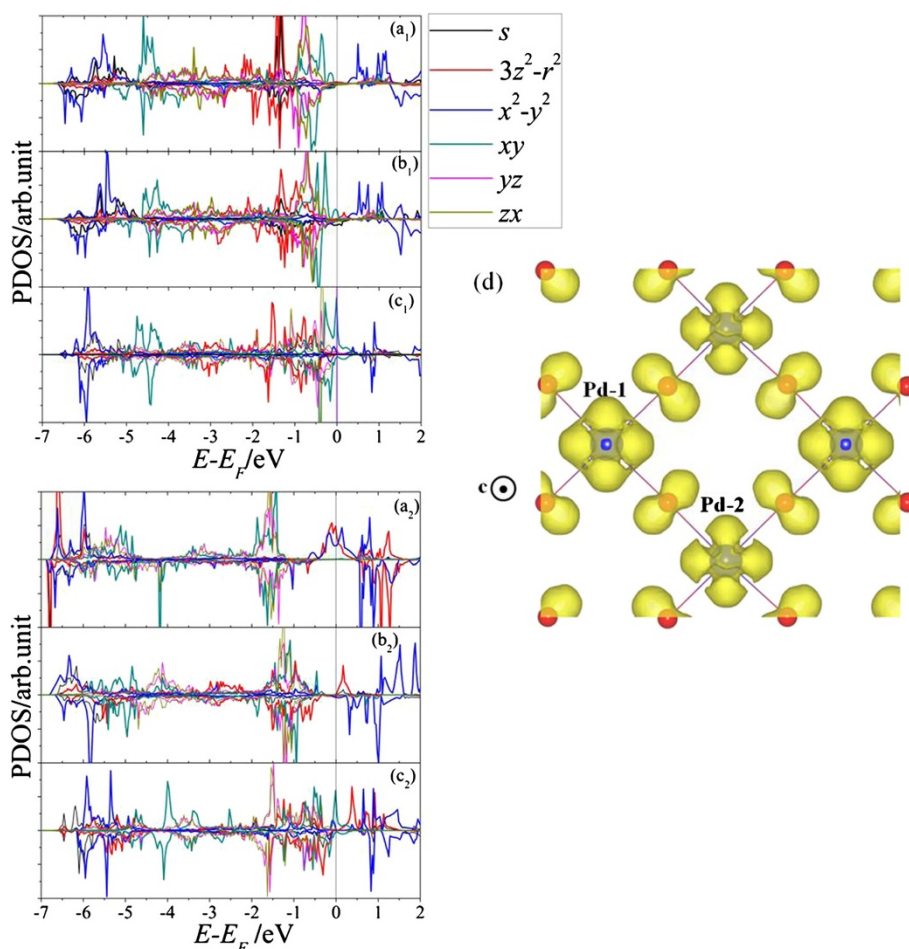


**Figure 3** Calculated projected density of states (PDOS) of two Pd atoms. Panels (a<sub>1</sub>) to (c<sub>1</sub>) are the PDOSs for Pd-1 located at the top-left site of Figure 2 group II (a) to (c). Panels (a<sub>2</sub>) to (c<sub>2</sub>) represent the PDOSs of Pd-2, which is located at the third  $FeO_2$  layer (a<sub>2</sub>), at the subsurface (b<sub>2</sub>), or the first  $FeO_2$  layer (c<sub>2</sub>). Positive (negative) values refer to spin-up (spin-down) states. The line through the zero point on the horizontal axis represents the Fermi level. (d) is the top view of the calculated isosurface of the partial charge density of the  $PdO_2$ -terminated surface containing  $V_O$  in the spin-up state in an energy window of (-0.1, 0.1) eV. The yellow-curved isosurfaces stand for the charge density of 0.6 a.u.<sup>-3</sup>.



atom at the second FeO<sub>2</sub> layer (Figure 2b), the change in PDOS of Pd-1 seems rather small and similar to that in panel (a<sub>1</sub>). However, the degeneracy of the *e<sub>g</sub>* state is lifted for Pd-2 because of the missing apical oxygen atom, leading to a downward shift in *d<sub>3z<sup>2</sup>-2</sub>* beneath the Fermi level, except for a small antibonding state near the Fermi level associated with hybridization between the Pd *d<sub>3z<sup>2</sup>-2</sub>* and *p* state of oxygen atom beneath it. The *t<sub>2g</sub>* states are also fully occupied in the form of a stable closed shell. The degeneracy of the *e<sub>g</sub>* state is lifted due to the lowering of symmetry at the surface for Pd-2 located at the first FeO<sub>2</sub> layer (Figure 2 group II (c)). However, as there is another O at the subsurface, a much stronger antibonding Pd *d<sub>3z<sup>2</sup>-2</sub>* state appears near the Fermi level in contrast to that in panel (b<sub>2</sub>). Additionally, the *d<sub>xy</sub>* state remarkably increases in energy due to increased hybridization between the Pd-*d<sub>xy</sub>* and O-*p<sub>y/x</sub>* states, and an especially sharp peak emerges at the Fermi level in the spin-up state. The Pd *d<sub>xy</sub>* state also appears near the Fermi level for Pd-1 as shown in panel (c<sub>1</sub>). The corresponding partial charge density for the peak at the Fermi level has been drawn on the (001) plane in panel (d). The spin-up partial charge density exhibits strong antibonding states in the form of *pdπ\** bonds between Pd and O in the energy window from -0.1 to +0.1 eV relative to the Fermi energy. As a result, the additional Pd at the neighboring surface site is less stable than that at the second FeO<sub>2</sub> layer.

Since V<sub>O</sub>s are more likely to form at the subsurface (LaO layer) than the surface in the Pd-containing FeO<sub>2</sub>-terminated surface, we placed another V<sub>O</sub> in the same LaO layer (Figure 2 group III (a) to (c)). If two V<sub>O</sub>s are both located at the subsurface, the second Pd atom tends to substitute the Fe atom either at the second FeO<sub>2</sub> layer forming a pair of Pd atoms (Figure 2 group III (b)) or on the surface forming the PdO<sub>2</sub> layer (Figure 2 group III (c)). The difference in energy between these two configurations is less than 0.05 eV. Thus, the additional V<sub>O</sub> stabilizes the PdO<sub>2</sub>-layer exposed to the vacuum.

Thus far, we have assumed the existence of V<sub>O</sub>. However, the concentration of V<sub>O</sub>s depends on their formation energy. Therefore, we have to verify the stability of surfaces containing V<sub>O</sub>(s) with different concentrations of Pd by taking the formation energy of V<sub>O</sub>s into account to further strengthen our conclusion. We calculated the relative energies of surfaces containing Pd<sub>*m*</sub>V<sub>O<sub>*n*</sub></sub> (*m* = 1 and 2 and *n* = 0, 1, and 2) relative to the perfect slab (without V<sub>O</sub>s) with Pd inside the bulk of LFO (see Figure 2 group I (a)). Note that the systems we have discussed here are surfaces with Pd atom(s) and V<sub>O</sub>(s) located on/near the surface. The relative energies ( $\Delta E^{\text{rel}}$ ) as a function of the chemical potential of oxygen ( $\Delta\mu_{\text{O}}$ ) are shown in Figure 4. The corresponding geometries

for the Pd<sub>*m*</sub>V<sub>O<sub>*n*</sub></sub>-containing surfaces are all included in Figure 2. Since two Pd atoms fail to segregate near/at the surface adjacently without V<sub>O</sub>s, the results for the Pd<sub>2</sub>-containing perfect surface excluded from Figure 4. The  $\Delta E^{\text{rel}}$  for each colored line is calculated as:

$$\begin{aligned} \text{Green line : } \Delta E^{\text{rel}} &= 2E_{\text{PdFeO}_4/(\text{LaO})_2/(\text{FeO}_2)_2/(\text{LaFeO}_3)_6}^{\text{tot}} - 2E_{\text{ref}}^{\text{tot}}, \end{aligned} \quad (1)$$

$$\begin{aligned} \text{Green line : } \Delta E^{\text{rel}} &= 2E_{\text{PdFeO}_4/\text{La}_2\text{O}_1/(\text{FeO}_2)_2/(\text{LaFeO}_3)_6}^{\text{tot}} - 2E_{\text{ref}}^{\text{tot}} \\ &+ 2\mu_{\text{O}}, \end{aligned} \quad (2)$$

$$\begin{aligned} \text{Pink line : } \Delta E^{\text{rel}} &= 2E_{\text{PdFeO}_4/\text{La}_2/(\text{FeO}_2)_2/(\text{LaFeO}_3)_6}^{\text{tot}} - 2E_{\text{ref}}^{\text{tot}} \\ &+ 4\mu_{\text{O}}, \end{aligned} \quad (3)$$

$$\begin{aligned} \text{Red line : } \Delta E^{\text{rel}} &= E_{\text{PdFeO}_4/\text{La}_2\text{O}_1/\text{PdFeO}_4/(\text{LaFeO}_3)_6}^{\text{tot}} \\ &+ E_{(\text{FeO}_2)_2/(\text{LaFeO}_3)_8}^{\text{tot}} - 2E_{\text{ref}}^{\text{tot}} + \mu_{\text{O}}, \end{aligned} \quad (4)$$

$$\begin{aligned} \text{Blue line : } \Delta E^{\text{rel}} &= E_{\text{PdFeO}_4/\text{La}_2/\text{PdFeO}_4/(\text{LaFeO}_3)_6}^{\text{tot}} \\ &+ E_{(\text{FeO}_2)_2/(\text{LaFeO}_3)_8}^{\text{tot}} - 2E_{\text{ref}}^{\text{tot}} + 2\mu_{\text{O}}, \end{aligned} \quad (5)$$

where the first items in Equations 1 to 5 on the right-hand side are the total energies of the Pd<sub>*m*</sub>V<sub>O<sub>*n*</sub></sub>-containing (*m* = 1 and 2 and *n* = 0, 1, and 2) surfaces, with their subscripts describing their compositions.  $E_{\text{ref}}^{\text{tot}}$

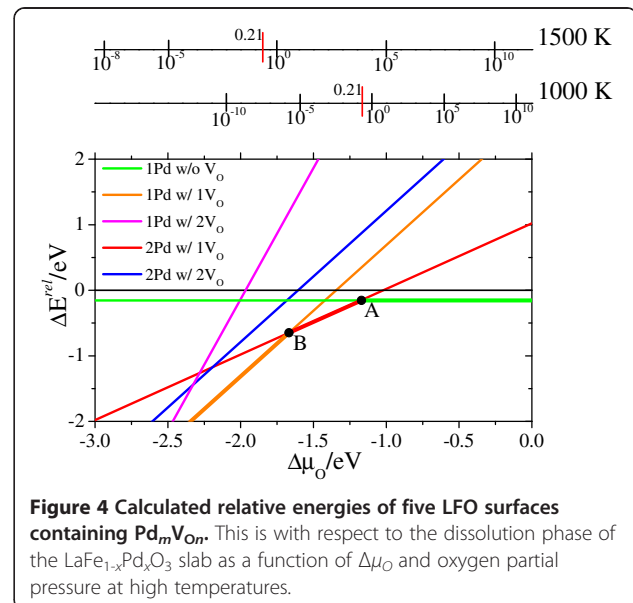


**Figure 4** Calculated relative energies of five LFO surfaces containing Pd<sub>*m*</sub>V<sub>O<sub>*n*</sub></sub>. This is with respect to the dissolution phase of the LaFe<sub>1-x</sub>Pd<sub>*x*</sub>O<sub>3</sub> slab as a function of  $\Delta\mu_{\text{O}}$  and oxygen partial pressure at high temperatures.

represents the total energy of the reference surface that contains one solid-solution state of Pd inside the bulk. The  $E_{(\text{FeO}_2)_2/(\text{LaFeO}_3)_8}^{\text{tot}}$  in Equations 4 and 5 is the total energy of the pristine  $\text{FeO}_2$ -terminated surface. The  $\mu_{\text{O}}$  is the chemical potential of oxygen. The chemical potentials of oxygen in the LFO bulk and gas phase are equal under equilibrium conditions. The  $\mu_{\text{O}}$  based on an ideal gas approximation is directly connected with the partial pressure ( $p(\text{O}_2)$ ) and temperature ( $T$ ) by

$$\mu_{\text{O}_2}^{\text{gas}}(T, p) = \mu_{\text{O}_2}^{\text{gas}}(T, p^0) + kT \ln \left( \frac{p}{p^0} \right), \quad (6)$$

$$\begin{aligned} \Delta\mu_{\text{O}}^{\text{gas}}(T, p) &= \frac{1}{2} \left( \mu_{\text{O}_2}^{\text{gas}}(T, p) - E_{\text{O}_2}^{\text{gas}} \right) \\ &= \Delta\mu_{\text{O}}^{\text{gas}}(T, p^0) + \frac{1}{2} kT \ln \left( \frac{p}{p^0} \right), \end{aligned} \quad (7)$$

in which  $k$  is the Boltzmann constant and  $p^0$  is taken to be the standard pressure.  $\mu_{\text{O}_2}^{\text{gas}}$  is the total energy of an isolated  $\text{O}_2$  molecule. The  $\Delta\mu_{\text{O}}^{\text{gas}}(T, p^0)$  item is determined by using thermodynamic data from the thermochemical tables [26]. Hence, we can obtain the formation energy of  $\text{V}_{\text{O}}(\text{s})$  based on Equations 2 to 5 by subtracting the item in Equation 1. As we assumed that the chemical potential of La would be very low in the present research, no metallic La or La oxides could precipitate on the surface although the La-O bonds were broken due to the formation of  $\text{V}_{\text{O}}\text{s}$  in the first LaO layer (Figures 2 groups II and III). According to the equations, the positive  $\Delta E^{\text{rel}}$  means the reference surface is more stable.

We can find from Figure 4 that when  $\Delta\mu_{\text{O}}$  is greater than -1.17 eV (point A), no  $\text{V}_{\text{O}}\text{s}$  form on the surface. The Pd-segregated surface (Figure 2 group I (b)) is slightly more stable than the surface with Pd inside the bulk of the perovskite (Figure 2 group I (a)). This indicates that Pd preferentially stays at the first layer of the LFO surface than the bulk position to some extent. One  $\text{V}_{\text{O}}$  in the surface appears at the subsurface (LaO layer) when  $\Delta\mu_{\text{O}}$  is lower than -1.17 eV. The surface containing  $\text{Pd}_2\text{V}_{\text{O}}$  is predicted to be stable between points A and B, indicating conditions with standard pressure at temperatures between 1,000 and 1,500 K. Two Pd atoms attract each other in such a surface by sharing one  $\text{V}_{\text{O}}$  in the first LaO layer (Figure 2 group II (b)). The  $\text{Pd}_1\text{V}_{\text{O}1}$ -containing surface (Figure 2 group II (n)) becomes dominant at  $\Delta\mu_{\text{O}}$  below -1.67 eV (point B) under standard pressure at temperatures over 1,500 K. Two  $\text{V}_{\text{O}}\text{s}$ -containing surfaces are predicted to be dramatically unstable compared with the other three surfaces due to the greater formation energy of two  $\text{V}_{\text{O}}\text{s}$  under the conditions given in Figure 4. The  $\text{Pd}_1\text{V}_{\text{O}2}$ -

containing surface (Figure 2 group III (d)) will appear under standard pressure at temperatures far above 1,500 K (the pink line: the critical point is beyond the scale of Figure 4). The surface containing  $\text{Pd}_2\text{V}_{\text{O}2}$  (Figure 2 group III (b)) for the blue line is predicted to be unstable under any conditions as presented in Figure 4. From what we have mentioned above, one  $\text{V}_{\text{O}}$  can be produced at the first LaO layer of the  $\text{FeO}_2$ -terminated surfaces with segregated  $\text{Pd}_m$  ( $m = 1$  and 2) under reasonable working conditions, and such surfaces are predicted to be dominantly stable over a wide range of  $\Delta\mu_{\text{O}}$ .

## Conclusions

We investigated what effect oxygen vacancies had on the tendency of additional Pd atoms to segregate at the  $\text{LaFe}_{1-x}\text{Pd}_x\text{O}_{3-y}$  surface, as well as compared the relative stability of  $\text{FeO}_2$ -terminated surfaces that contained  $\text{Pd}_m\text{V}_{\text{O}n}$  versus the oxygen chemical potential, by using first-principles theoretical calculations. We pointed out that Pd atoms repulse one another without  $\text{V}_{\text{O}}\text{s}$ . However, if there are  $\text{V}_{\text{O}}\text{s}$  at the subsurface layer, Pd atoms become attractive, forming a pair of Pd atoms while sharing one  $\text{V}_{\text{O}}$ . Furthermore, we clarified that the  $\text{FeO}_2$ -terminated surface containing  $\text{Pd}_m\text{V}_{\text{O}}$  could be predicted to become stable over a wide range of oxygen chemical potentials below -1.17 eV. Therefore, the present results provide support that the calcination of precious metals containing catalysts at 1,073 K or high temperatures in air during the catalyst preparation step leads to the formation of oxygen vacancies near the surface and then enhances the formation of a  $\text{LaPdO}_{3-y}$  layer in the vicinity of the  $\text{LaFeO}_3$  oxide surface.

## Competing interests

The authors declare that they have no competing interests.

## Authors' contributions

ZT, AU, IH, and SY carried out calculations with the help of HK and KI and drafted the manuscript. YM participated in the design of the study and helped to draft the manuscript. All authors read and approved the final manuscript.

## Acknowledgments

The present work was partly supported by a Ministry of Education, Culture, Sports, Science and Technology (MEXT) program called the "Elements Strategy Initiative to Form Core Research Center" (since 2012). The Advanced Institute for Materials Research (AIMR) was established by the World Premier Research Center Initiative (WPI), MEXT, Japan. The calculations were done at the supercomputer centers of Osaka University, the Institute for Solid State Physics, the University of Tokyo, and Tohoku University.

## Author details

<sup>1</sup>Division of Precision Science & Technology and Applied Physics, Graduate School of Engineering, Osaka University, 2-1, Yamada-oka, Suita, Osaka 565-0871, Japan. <sup>2</sup>Institute of Scientific and Industrial Research, Osaka University, 8-1 Mihogaoka, Ibaraki, Osaka 567-0047, Japan. <sup>3</sup>Advanced Institute for Materials Research (AIMR), Tohoku University, Sendai 980-8577, Japan. <sup>4</sup>Department of Physics and Earth Science, Faculty of Science, University of the Ryukyus, 1 Senbaru, Nishihara, Okinawa 903-0213, Japan. <sup>5</sup>Elements Strategy Initiative for Catalysts and Batteries (ESICB), Kyoto University, Katsura, Kyoto 615-8520, Japan.

Received: 31 December 2012 Accepted: 21 March 2013  
Published: 1 May 2013

## References

- Nishihata Y, Mizuki J, Akao T, Tanaka H, Uenishi M, Kimura M, Okamoto T, Hamada N: **Self-regeneration of a Pd-perovskite catalyst for automotive emissions control.** *Nature* 2002, **418**:164–167.
- Tanaka H, Uenishi M, Taniguchi M, Tan I, Narita K, Kimura M, Kaneko K, Nishihata Y, Mizuki J: **The intelligent catalyst having the self-regenerative function of Pd, Rh and Pt for automotive emissions control.** *Catal Today* 2006, **117**:321–328.
- Tanaka H, Taniguchi M, Uenishi M, Kajita N, Tan I, Nishihata Y, Mizuki J, Narita K, Kimura M, Kaneko K: **Self-regenerating Rh- and Pt-based perovskite catalysts for automotive-emissions control.** *Angew Chem Int Ed* 2006, **45**:5998–6002.
- Sato N, Tanaka H, Tan I, Uenishi M, Kajita N, Taniguchi M, Narita K, Kimura M: **Research on the co-free intelligent catalyst.** In *Proceedings of the SAE 2003 World Congress & Exhibition: March 3, 2003*. Detroit. Warrendale: SAE International; 2003.
- Tanaka H, Taniguchi M, Kajita N, Uenishi M, Tan I, Sato N, Narita K, Kimura M: **Design of the intelligent catalyst for Japan ULEV standard.** *Topics Catal* 2004, **30**:31:389.
- Uenishi M, Taniguchi M, Tanaka H, Kimura M, Nishihata Y, Mizuki J, Kobayashi T: **Redox behavior of palladium at start-up in the perovskite-type LaFePdOx automotive catalysts showing a self-regenerative function.** *Appl Catal Environ* 2005, **57**:267–273.
- Eyssler A, Mandaliev P, Winkler A, Hug P, Safonova O, Figi R, Weidenkaff A, Ferri D: **The effect of the state of Pd on methane combustion in Pd-doped LaFeO<sub>3</sub>.** *J Phys Chem C* 2010, **114**:4584.
- Eyssler A, Winkler A, Mandaliev P, Hug P, Weidenkaff A, Ferri D: **Influence of thermally induced structural changes of 2 wt% Pd/LaFeO<sub>3</sub> on methane combustion activity.** *Appl. Catal. B: Environ.* 2011, **106**:494–502.
- Eyssler A, Winkler A, Nachttegaal M, Matam SK, Hug P, Safonova O, Weidenkaff A, Ferri D: **On the state of Pd in Perovskite-type oxidation catalysts of composition A(B, Pd)O<sub>3±δ</sub> (A = La, Y; B = Mn, Fe, Co).** *Chem Mater* 2012, **24**:1864–1875.
- Hamada I, Uozumi A, Morikawa Y, Yanase A, Katayama-Yoshida H: **A density functional theory study of self-regenerating catalysts LaFe<sub>1-x</sub>M<sub>x</sub>O<sub>3-y</sub> (M = Pd, Rh, Pt).** *J Am Chem Soc* 2011, **133**:18506–18509.
- Katz M, Graham G, Duan Y, Liu H, Adamo C, Schlom D, Pan X: **Self-regeneration of Pd-LaFeO<sub>3</sub> catalysts: new insight from atomic-resolution electron microscopy.** *J Am Chem Soc* 2011, **133**:18090–18093.
- Kizaki H, Kusakabe K, Nogami S, Katayama-Yoshida H: **Generation of nano-catalyst particles by spinodal nano-decomposition in perovskite.** *Appl Phys Express* 2008, **1**:104001.
- Tian ZX, Inagaki K, Morikawa Y: **Density functional theory on the comparison of the Pd segregation behavior at LaO- and FeO<sub>2</sub>-terminated surfaces of LaFe<sub>1-x</sub>Pd<sub>x</sub>O<sub>3-y</sub>.** *Current Appl Phys* 2012, **12**:S105.
- Morikawa Y, Ishii H, Seki K: **Theoretical study of n-alkane adsorption on metal surfaces.** *Phys Rev B* 2004, **69**:041403.
- Sawada H, Morikawa Y, Terakura K, Hamada N: **Jahn-Teller distortion and magnetic structures in LaMnO<sub>3</sub>.** *Phys Rev B* 1997, **56**:12154–12160.
- Giannozzi P, Baroni S, Bonini N, Calandra M, Car R, Cavazzoni C, Ceresoli D, Chiarotti GL, Cococcioni M, Dabo I, Corso AD, Gironcoli S, de Fabris S, Fratesi G, Gebauer R, Gerstmann U, Gougoussis C, Kokalj A, Lazzeri M, Martin-Samos L, Marzari N, Mauri F, Mazzaarello R, Paolini S, Pasquarello A, Paulatto L, Sbraccia C, Scandolo S, Sclauzero G, Seitsonen AP, Smogunov A, Umari P, Wentzcovitch RM: **QUANTUM ESPRESSO: a modular and open-source software project for quantum simulations of materials.** *J Phys Condens Matter* 2009, **21**:395502.
- Vanderbilt D: **Soft self-consistent pseudopotentials in a generalized eigenvalue formalism.** *Phys Rev B* 1990, **41**:7892–7895.
- Perdew JP, Burke K, Ernzerhof M: **Generalized gradient approximation made simple.** *Phys Rev Lett* 1996, **77**:3865.
- Barbier A, Stierle A, Kasper N, Guittet M-J, Jupille J: **Surface termination of hematite at environmental oxygen pressures: Experimental surface phase diagram.** *Phys Rev B* 2007, **75**:233406.
- Shivakumara C: **Low temperature synthesis and characterization of rare earth orthoferrites LnFeO<sub>3</sub> (Ln=La, Pr and Nd) from molten NaOH flux.** *Solid State Commun* 2006, **139**:165.
- Lee CW, Behera RK, Wachsman ED, Phillpot SR, Sinnott SB: **Stoichiometry of LaFeO<sub>3</sub> (010) surface determined from first-principles and thermodynamic calculations.** *Phys Rev B* 2011, **83**:115418.
- Giraudon J-M, Elhachimi A, Wyrwalski F, Siffert S, Aboukais A, Lamonier J-F, Leclercq G: **Studies of the activation process over Pd perovskite-type oxides used for catalytic oxidation of toluene.** *Appl Catal B: Environmental* 2007, **75**:157.
- Miquel P, Yamin Y, Lombaert K, Dujardin C, Granger P: **Thermal ageing induced effects on Pd/LaFeO<sub>3</sub> for NOx reduction by hydrocarbons: influence of the preparation method.** *Top Catal* 2009, **52**:1791.
- Humphrey W, Dalke A, Schulten K: **VMD: visual molecular dynamics.** *J Mol Graphics* 1996, **14**:33.
- Monkhorst HJ, Pack JD: **Special points for Brillouin-zone integrations.** *Phys Rev B* 1976, **13**:5188.
- Linstrom PJ: *Mallard WG (Eds): NIST Chemistry WebBook, NIST Standard Reference Database No. 69*. National Institute of Standards and Technology: Gaithersburg, MD; 2003.

doi:10.1186/1556-276X-8-203

**Cite this article as:** Tian et al.: First-principles investigation on the segregation of Pd at LaFe<sub>1-x</sub>Pd<sub>x</sub>O<sub>3-y</sub> surfaces. *Nanoscale Research Letters* 2013 **8**:203.

**Submit your manuscript to a SpringerOpen<sup>®</sup> journal and benefit from:**

- Convenient online submission
- Rigorous peer review
- Immediate publication on acceptance
- Open access: articles freely available online
- High visibility within the field
- Retaining the copyright to your article

Submit your next manuscript at ► [springeropen.com](http://springeropen.com)